Annu. Rev. Mater. Sci. 2000. 30:523–43
Copyright © by Annual Reviews. All rights reserved

MECHANISMS FOR ENHANCED FORMATION OF THE C54 PHASE OF TITANIUM SILICIDE ULTRA-LARGE-SCALE INTEGRATION CONTACTS

J. M. E. Harper, C. Cabral, Jr., and C. Lavoie
IBM T. J. Watson Research Center, Yorktown Heights, New York 10598; e-mail: jmharper@us.ibm.com

Key Words low resistivity, disilicide, transition metal, ion implantation, alloy

■ **Abstract** Three methods have recently been developed to enhance the formation of the low-resistivity C54 phase of $TiSi_2$, the most widely used silicide contact in ultra-large-scale integration devices. These methods are (*a*) ion implantation of a transition metal into the Si before Ti deposition; (*b*) deposition of a thin transition metal interlayer between the Si and Ti; and (*c*) codeposition of Ti alloyed with a transition metal. Each of these methods decreases the C49-to-C54 transformation temperature by >100°C and improves the probability of phase formation in narrow lines by increasing the nucleation site density. In this paper, we identify the aspects of phase formation that are shared by these three methods, review the methodology by which they were developed, and summarize the applications to silicon devices. Mechanisms that are responsible for the enhanced formation of C54 $TiSi_2$ are reviewed, based on a combination of temperature-controlled in situ measurements of resistance, X-ray diffraction, and optical scattering, coupled with ex situ studies of phase formation and morphology. The main mechanisms are identified as enhanced nucleation of the C54 phase by a reduction of grain size in the C49 phase and the creation of crystallographic templates of the C40 disilicide phase and the metal-rich Ti_5Si_3 phase.

INTRODUCTION

Titanium disilicide ($TiSi_2$) is the most widely used silicide for making low-resistivity contacts to silicon in ultra large-scale integration (ULSI) devices. One of its advantages is the ability to form the silicide selectively on exposed silicon surfaces, allowing the use of the self-aligned silicide (salicide) process (1). The process sequence is outlined in Figure 1, which shows a schematic cross section of a complementary metal-oxide-semiconductor (CMOS) transistor. After the exposed silicon surfaces are cleaned, a blanket thin film of Ti is deposited, usually by sputtering. Next, an annealing treatment at >500°C in nitrogen is applied to react the Ti with the exposed Si and form the precursor phase C49 $TiSi_2$, which has a relatively high resistivity (50–75 $\mu\Omega$-cm). A surface layer of TiN forms simultaneously.

0084-6600/00/0801-0523$14.00

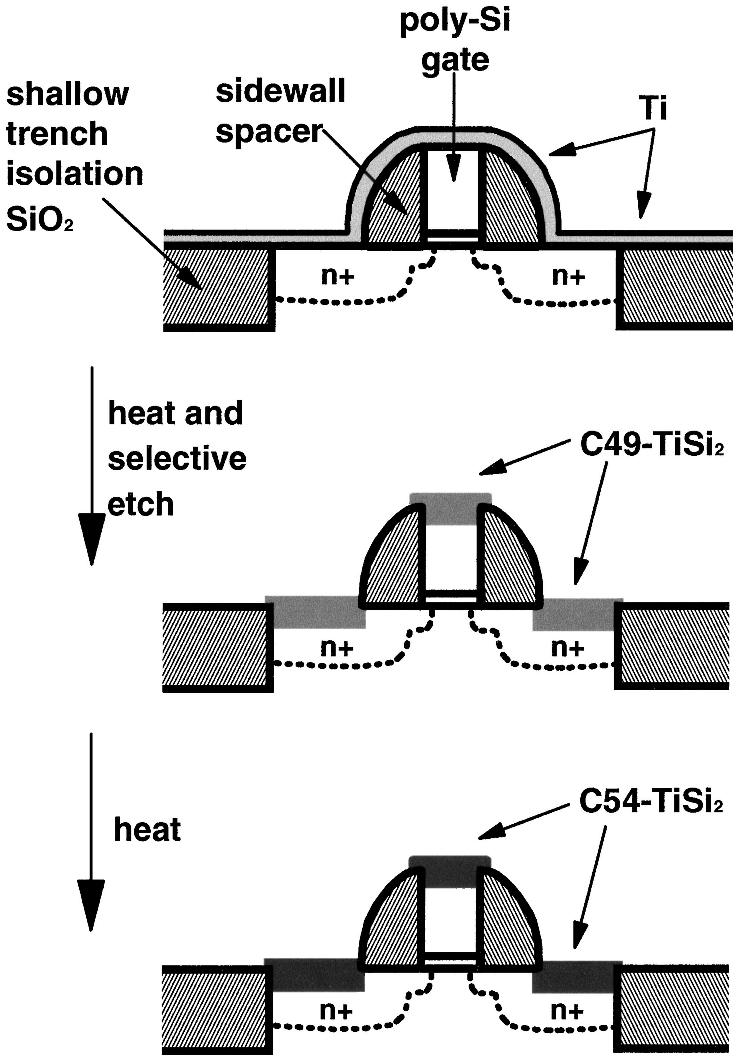

Figure 1 Cross-section schematic diagram of a CMOS transistor showing the salicide process sequence.

Areas of Ti and TiN that did not react with Si are removed with a selective chemical etch, followed by a second heat treatment at >700°C to transform the C49 $TiSi_2$ phase into the desired low-resistivity C54 $TiSi_2$ phase (15–20 $\mu\Omega$-cm). The success of this process depends on obtaining the C49-to-C54 transformation everywhere across a patterned silicon wafer, in features ranging in size down to short, isolated lengths with the minimum line width. A 200-mm-diameter silicon wafer processed with 0.25-μm line width CMOS technology has many millions

of transistors per square centimeter, with the wafer diameter expected to increase to 300 mm in the near future along with continued reduction in line width. These trends are recognized by the Semiconductor Industry Association [SIA (2)], which identifies "junction scaling with low resistance contacts" as one of the difficult challenges facing the industry during the next 5 years. The SIA states that "producing highly doped and fully activated shallow junctions contacted with low sheet resistance materials will challenge the silicide process and the allowable thermal budget" (2).

The ability to manufacture $TiSi_2$ contacts was not well developed until the existence of the C49 phase as a precursor to the formation of C54 $TiSi_2$ was recognized in the mid-1980s (3, 4). However, as CMOS technology evolved through the late 1980s and early 1990s to line widths of <0.5 μm, it was found that the C49-to-C54 transformation did not reliably occur in the smallest features, leading to a narrow line effect in which bimodal resistance distributions were encountered with decreasing line width. A bimodal resistance distribution is caused by having both lines with low-resistivity C54 $TiSi_2$ and lines with high-resistivity C49 $TiSi_2$ present in the same sample of tested lines. Figure 2 is a schematic diagram showing both C54 and C49 grains on poly-Si and single-crystal Si (x-Si) contact regions of a CMOS transistor. If a large fraction of C49 grains is present in the silicide capping a poly-Si line, that line will not have as low a resistance as a line capped entirely with C54 grains. Because circuit designs must allow for signal propagation along the slowest paths, the presence of the high-resistivity C49 phase can limit the performance of the entire chip (5). Lasky et al (6) identified the problem as an inadequate density of nucleation sites in small features, and they estimated the site density to be <0.05 sites/μm^2. Underlying this poor nucleation

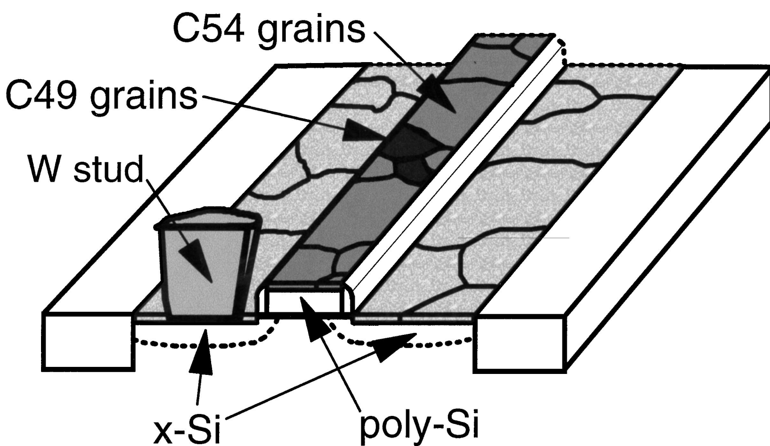

Figure 2 Schematic diagram of the silicide contacts on a CMOS transistor showing regions containing C54 and C49 $TiSi_2$ grains.

density is the small free-energy difference between the C49 and C54 $TiSi_2$ phases, estimated to be ~50 meV/atom (7). Also, this transformation has been found to have a high activation energy, >4 eV, depending on the dopants and crystallinity of the Si (8). Several methods for influencing the transformation were identified, including rapid thermal annealing (9, 9a), addition of Sb to codeposited $TiSi_2$ (10), addition of Sn to Ti (11), and preamorphization of Si by ion implantation of Xe (12) or As (13). However, each method had limitations. Also, other efforts to enhance the formation of C54 $TiSi_2$ by ion bombardment were unsuccessful and often caused a delay in C54 formation to higher temperatures (14).

In the early 1990s, the beneficial effect on C54 formation of ion-implanting molybdenum into Si before Ti deposition was discovered by an IBM research and development team (15, 15a), prompting a thorough examination of the effects of transition metal additives on the C49-to-C54 transformation. From this study, three methods were developed for enhancing the C49-C54 transformation in narrow lines, each involving the addition of transition metals at low concentrations: (*a*) ion implantation of a transition metal into the Si before Ti deposition, (*b*) deposition of a thin transition metal interlayer between the Si and the Ti, and (*c*) codeposition of Ti alloyed with a transition metal. The three methods have in common an increased density of nucleation sites for the transformation, and, in several cases, evidence has been found for a template effect caused by the formation of silicide phases with crystallographic similarities to the desired C54 $TiSi_2$ phase. To evaluate the large number of choices for an additive element, it was necessary to develop methods to rapidly gather information from a wide range of compositions, heat treatments, substrate types (single-crystal or polycrystalline Si), dopant types (B, P, or As), dopant concentrations, and line widths. In this review, we describe the experimental methods for evaluating this large range of samples, summarize the findings for the three methods of enhancing C54 formation, and discuss the mechanisms and implications for future control of thin-film silicide phases.

EXPERIMENTAL METHODS

Thin Film Deposition and Ion Implantation

Ion implantation of several transition metals into Si before Ti deposition was studied to determine the values of dose and energy that cause a substantial lowering of the C49-to-C54 transformation temperature. Examples given by Mann et al (15, 15a) include Mo and W implanted at 45 keV with doses in the range 10^{13}–10^{14} ions/cm^2. In most cases, the Si was annealed before Ti deposition, simulating a junction activation annealing. Promising results from this study stimulated a broader survey of transition metals that involve evaporation and sputtering to deposit an interlayer on the Si before Ti deposition.

Interlayer deposition was carried out initially with an electron beam evaporator with a base pressure of ~10^{-5} Pa and deposition rates of typically 0.1 nm/s. The

Si surface was precleaned with a dilute HF solution immediately before samples were loaded into the evaporation chamber. Samples of single-crystal Si(100) were used with various dopants, together with samples on which poly-Si was deposited on 300 nm of SiO_2 to electrically isolate the silicide from the Si(100) substrate. Deposition of a transition metal interlayer of thickness 0.1–5 nm was immediately followed by a Ti layer of thickness 20–60 nm. Promising choices were further studied by using sputter deposition in a planar magnetron deposition system with a base pressure of $\sim 10^{-5}$ Pa, Ar sputtering gas pressure of typically 1.3 Pa, and deposition rates of $\sim$0.01 nm/s for the interlayer and 0.2 nm/s for the Ti. As it became clear that the optimal interlayer thicknesses were only a few monolayers (16–18), a parallel study was undertaken to deposit alloys of Ti with transition metals by using both coevaporation and cosputtering.

Alloy deposition by cosputtering was performed in an ultra-high vacuum (UHV) system with a base pressure of $\sim 10^{-7}$ Pa, dual 7.5-cm-diameter dc planar magnetron sources, Ar sputtering gas pressure of 0.53 Pa, and deposition rates of 0.001–0.025 nm/s for the alloying element and 0.15 nm/s for the Ti (19). The ability to deposit a wide range of alloy compositions onto samples rapidly introduced through a multiwafer loadlock proved to be essential in gaining a broad understanding of the dependence of the C49-to-C54 transformation on the choice of the additive metal and on the alloy composition. For most alloys, substrates of both single-crystal Si(100) and poly-Si with various dopants were used, together with sets of patterned narrow-line samples, which are described below. This approach enabled large numbers of samples to be processed and evaluated by the rapid analytical methods described below. The combination of rapid synthesis and rapid turnaround analysis enabled a rate of progress that would have been unattainable with traditional experimental methods and schedules.

Fabrication of Patterned Samples

Samples with a range of line widths and line lengths were fabricated to study the dependence of the C49-to-C54 transformation on both line width and area. Both single-crystal Si(100) and poly-Si samples were prepared, as shown in Figure 3. The single-crystal Si samples (Figure 3*a*) were prepared by patterning lines of SiO_2, then adding SiO_2 sidewalls to control the width of the exposed surface of Si(100), thereby defining the width of the Si for reaction with the deposited metal. These samples resembled the source and drain contact regions of a CMOS transistor. The poly-Si samples (Figure 3*b*) were prepared by using the same sequence as a gate conductor process for a CMOS transistor; however, for these experiments, no silicon device structures were needed below the poly-Si lines. The exposed top surface of the poly-Si lines provided an Si surface for reaction with the metal films that were deposited as a blanket coating. Lines ranging in width from 0.1 to 2.0 μm were prepared, using X-ray lithography at the IBM Advanced Lithography Facility, and line lengths were defined by cutting the narrow lines with a set of orthogonal lines patterned by optical lithography. This hybrid lithographic

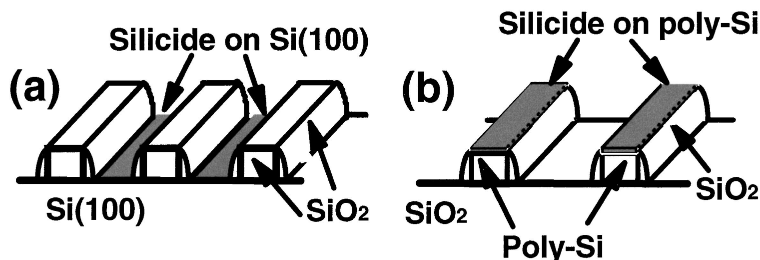

Figure 3 Samples used to study silicide formation on isolated narrow-line regions of (*a*) Si(100) and (*b*) poly-Si.

approach provided rectangular arrays of several-millimeter dimensions with specified line widths and areas, with each array large enough for analysis by X-ray and optical-scattering measurements to monitor the evolution of the silicide phases. Typically, the patterned line samples underwent the first annealing treatment to form C49 $TiSi_2$, followed by selective chemical etching to define the narrow lines and to remove excess metal. The subsequent evolution of phases was then monitored on each array as needed to determine the dependence on line width and area. With blanket samples, the entire phase formation sequence could be followed beginning at room temperature.

Temperature-Ramped and Isothermal In Situ Analysis

Temperature-ramped sheet resistance measurements were carried out by a four-point probe method during annealing at rates of 0.17–3.0°C/s from 20°C to 900°C in purified He or in N_2. X-ray measurements of crystal structures at room temperature were made using the Bragg-Brentano configuration with $Cu_{K\alpha}$ radiation (λ = 0.15405 nm). Temperature-ramped measurements were made using synchrotron X-ray radiation (20) on the IBM/MIT beamline X20C at the National Synchrotron Light Source, Brookhaven National Laboratory, which is shown schematically in Figure 4. In this system, the X-ray wavelength λ is 0.1797 nm, photon flux is 0.3×10^{13}–1.0×10^{13} photons/s, and measurements of scattered X-ray intensities are obtained by using a linear detector that covers a 2θ angular range of 10°. The linear detector contained 1024 diodes in the 10° angular range, from which the signals were collected in groups of 8, giving 128 data points per measurement. Each of these measurements was made several times per second for a total of 600 measurements during temperature ramping or isothermal studies, providing an almost continuous record of the evolving crystal phases. The sample temperature was calibrated by using the eutectic melting temperatures of Al-Si, Au-Si, and Ag-Si. In addition to sheet resistance and X-ray scattering, simultaneous measurement of optical diffuse scattering was made to detect changes in surface roughness or optical constants. This measurement provided additional sensitivity to small changes in sample properties. An He-Ne laser beam was focused on the sample

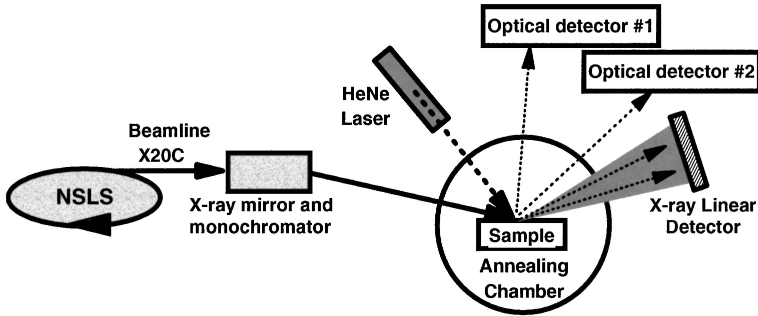

Figure 4 Schematic diagram of the synchrotron X-ray analysis system at the National Synchrotron Light Source, beamline X20C.

area, and the scattered intensity was measured at two nonspecular angles to provide information on surface roughness at two spatial wavelengths, 0.5 and 5.0 μm.

Microstructure and Composition Measurements

A significant finding early in our study of silicide phase formation was that the crystallographic texture of the reacted silicides has a strong dependence on film thickness and on the dimensions of patterned lines. Rather than being randomly oriented, the silicide grains often have a strong fiber texture, in which one crystal axis is strongly aligned perpendicular to the sample surface. Additionally, in narrow lines, silicide grains may also have a strong in plane alignment relative to the narrow-line dimensions. To quantify these effects, X-ray pole figure measurements were made with a Schultz geometry in which the sample is rotated and tilted through a range of orientations while the intensity of a chosen X-ray diffraction peak is measured. The result is a map of the scattering intensity of this set of lattice planes relative to the sample orientation. Both a rotating anode $Cu_{K\alpha}$ source and the synchrotron X-ray source at the National Synchrotron Light Source were used to obtain texture information. Beamline X20A was also used with an NaI detector, and some texture measurements were made using a charge-coupled device area detector, enabling simultaneous observation of the evolution of several texture components.

The crystal phases present in annealed samples could be identified by X-ray diffraction, but additional microscopic studies were required to determine the physical relationship and morphology of these phases. Transmission electron microscopy (TEM) was used in bright-field, convergent-beam, and selected area diffraction modes, with a Philips CM-30 SuperTwin TEM (21). Phase identification was confirmed by both standard X-ray diffraction patterns (22) and electron diffraction simulations (23). The propagation speed of the C49-to-C54 transformation front was also measured in several blanket and patterned samples, using a temperature-controlled heating stage in a JEOL 4000-FX TEM (24). The compositions

of films containing interlayers and alloy elements were measured by Rutherford backscattering spectroscopy, and local compositional variations were determined using energy dispersive X-ray spectroscopy on a Philips CM-20 field emission TEM/STEM (21).

RESULTS

Ion Implantation into Silicon before Titanium Deposition

A reduction of the C54 $TiSi_2$ formation temperature by 100–150°C was obtained by implanting Mo into poly-Si before Ti deposition and using a dose of 1×10^{13} ions/cm^2 at 45 keV and a Ti thickness of 25–55 nm (15, 15a). The sheet resistance as a function of temperature is shown in Figure 5 for blanket samples with and without the Mo implant, heated at 0.25°C/s. Without the Mo implant, a resistance plateau is clearly visible in the temperature range 700–780°C, which has been shown to be characteristic of the C49 $TiSi_2$ phase (1). The transformation to C54 $TiSi_2$ is signaled by the resistance decrease at 780°C. With the Mo implant, there is no distinct plateau, and the low resistance indicates that C54 $TiSi_2$ has formed at a lower temperature than without the implant. X-ray diffraction measurements on samples quenched from 700°C confirmed that the Mo implant enables the formation of the C54 phase at 700°C, whereas at this temperature, the sample without the Mo implant is still in the C49 phase.

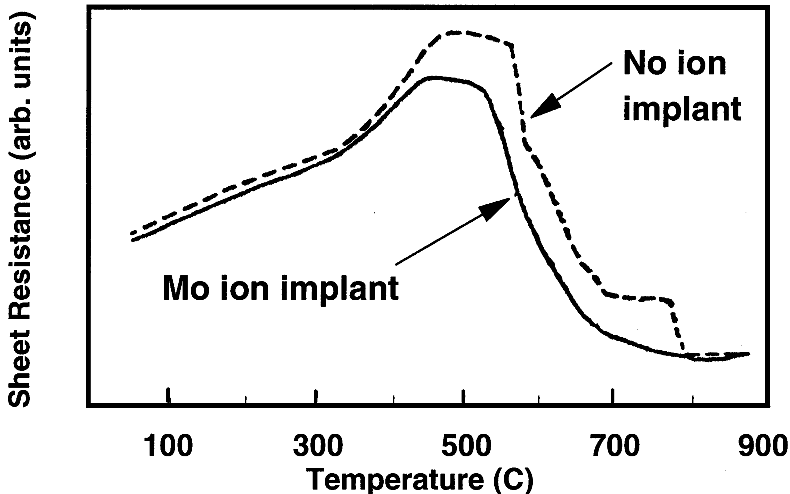

Figure 5 In situ sheet resistance versus temperature for Ti/Si samples with and without Mo implanted into the Si (15, 15a).

The improvement in C54 formation observed in blanket samples was also demonstrated in patterned samples of n^+ poly-Si with 0.4-μm line widths (15, 15a) by measuring the sheet resistance of the lines with and without Mo implants, after a 650°C, 30-min annealing. The implanted samples had a uniformly low sheet resistance that is characteristic of the C54 phase, whereas the unimplanted samples had a wide distribution of sheet resistances even after an additional annealing at 825°C, indicating incomplete transformation to the C54 phase. These results were obtained by annealing the implanted Si before Ti deposition at 900°C in N_2, simulating a junction activation annealing. This step differentiates this approach from implanting to preamorphize the Si (25, 25a, 25b) and from ion mixing of an existing Ti/Si interface (26). TEM measurements of the C54 grain size indicated a >100-fold increase in the C54 nucleation density for the Mo-implanted samples compared with unimplanted samples (15, 15a). Similar results were obtained on p^+-doped poly-Si lines, and some enhancement of C54 formation was obtained with W implantation. The enhancement of C54 formation by Mo ion implantation has been confirmed by other researchers, in some cases with a preamorphization implant of As or Ge (25, 25a, 25b).

Interlayer Deposition between Silicon and Titanium

After the demonstration of C54 enhancement by Mo and W ion implantation, the deposition of a thin interlayer of Mo or W between Si and Ti was soon shown to provide a similar enhancement of C54 formation (16, 18). An example is given in Figure 6, which shows the sheet resistance of 32-nm-thick sputtered Ti on poly-Si vs temperature for samples with and without a Mo interlayer <3 nm thick (18). As for Ti on Mo-implanted Si (Figure 5), the transformation to low-resistivity C54 $TiSi_2$ occurs at a temperature ~100°C lower with the Mo interlayer, compared with pure Ti/Si. In addition, the formation of the C49 $TiSi_2$ phase is shifted 30°C–50°C higher when an Mo interfacial layer is used. The flexibility of thin-layer deposition by evaporation or sputtering enabled a rapid survey of candidate interlayer elements for the enhancement of C54 formation. Cabral et al (18) demonstrated that a Mo interlayer <3 nm thick decreased the C54 formation temperature by ~100°C and also enabled the transformation to occur in patterned poly-Si lines with line widths of 0.25–1.0 μm after a rapid thermal annealing to 700°C for 30 s in N_2, for which pure Ti/Si samples remained in the C49 phase (27). However, it was found that the optimal interlayer thickness for C54 enhancement with various metals was typically in the range of several monolayers (18). This result has been confirmed for Mo by several other researchers, both with (28) and without (16, 29) preimplantation. The atom spacing in the (003) planes of the C40 (Ti-Mo)Si_2 structure was noted as being close to the spacing in the (040) planes of the C54 $TiSi_2$ structure (<3% mismatch), suggesting a crystallographic template mechanism that enhances C54 formation (16). Ta was also found to behave in a similar manner to Mo (16), and the lattice spacing for C40 $TaSi_2$ is a close match to C54 $TiSi_2$ (<0.3%

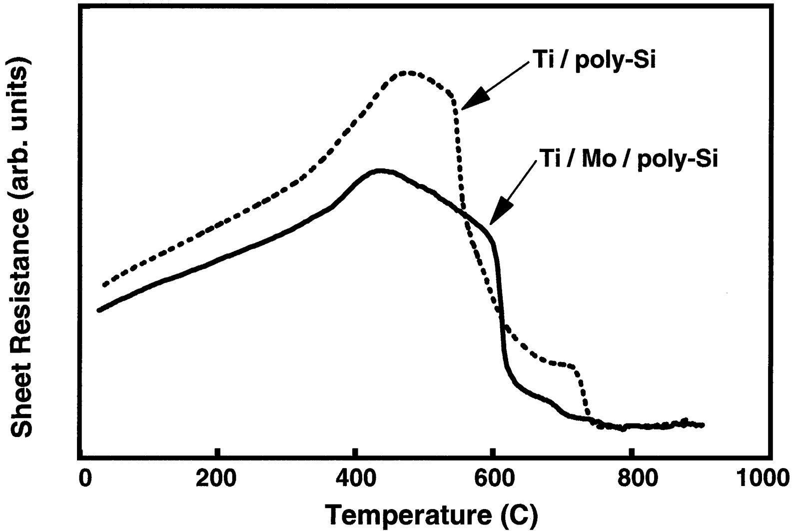

Figure 6 In situ sheet resistance versus temperature for 32-nm-thick Ti on poly-Si with and without a Mo interlayer (18).

mismatch) (17). In a microstructural study of the Ti/Mo/Si interlayer system by Quintero et al (30), the metal-rich silicide Ti_5Si_3 was observed to form at temperatures lower than the C54 $TiSi_2$ phase, prompting the additional suggestion of a template relationship between the (300) planes of the Ti_5Si_3 structure and the (040) planes of the C54 $TiSi_2$ structure and/or the (003) planes of the C40 structure (30).

Titanium Alloy Deposition onto Silicon

The reduction of the C54 transformation temperature with codeposited Ti alloys was first demonstrated by Cabral et al (19) for the alloying elements Mo, Ta, and Nb. As with the methods of ion implantation and interlayer deposition, decreases in the transformation temperature by $>100°C$ were obtained by using compositions of 1–20 at% alloying element codeposited with Ti. An example of the sheet resistance vs temperature for Ti(Ta) alloys reacted with poly-Si is shown in Figure 7 (19), and the in situ X-ray diffraction analysis obtained during temperature ramping for these compositions is shown in Figure 8 (19), which identifies the positions of several diffraction peaks. The decrease in C54 formation temperature with increasing alloying element concentration was found to be quite similar for Ta and Nb, as shown in Figure 9. However, the resistivity as a function of concentration for Mo differed from the behavior of Ta and Nb, as shown in Figure 10. The C54 formation behavior in narrow patterned lines was examined for Ti(Ta) alloys

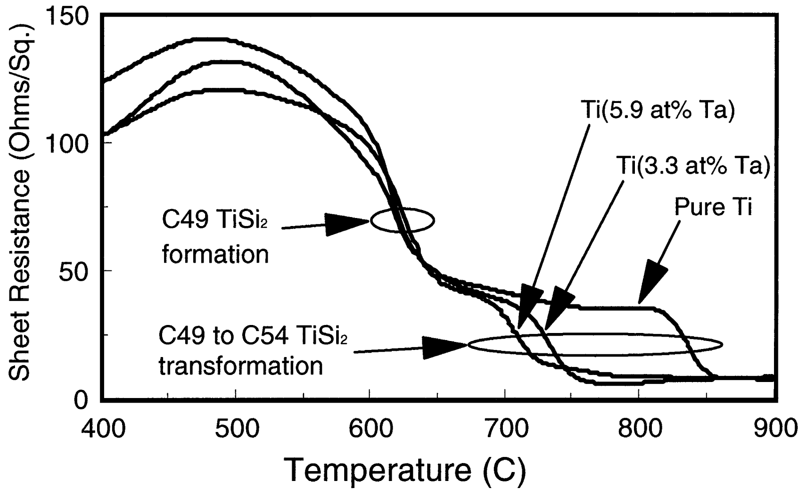

Figure 7 In situ sheet resistance versus temperature for Ti(Ta) alloys on poly-Si with concentrations of 0, 3.3, and 5.9 at% Ta (19).

with both Si(100) and poly-Si substrates. An example is shown in Figure 11 for pure Ti and for Ti(Ta) on patterned line widths ranging from 0.13 to 0.56 μm in addition to blanket samples (19). The Ti(Ta) alloy consistently forms C54 $TiSi_2$ at temperatures that are ~100°C lower than those required with pure Ti, even at line widths approaching 0.1 μm.

Because X-ray diffraction reveals the presence of crystalline phases, but does not indicate their physical relationship, TEM studies of microstructures and local compositions have been essential in obtaining direct evidence for the interactions between the precursor phases (C49, C40, and metal-rich silicides) and the final C54 phase. Quintero et al (21) have examined the reaction of Ti (5.9 at% Ta) with silicon and found the sequence of phase evolution to be quite subtle. A Ti(Ta) thickness of 32 nm was deposited on Si(100) and annealed at 3°C/s in N_2, with multiple samples quenched from various temperatures to examine the phase formation sequence. The appropriate quench temperatures were determined from prior temperature-ramped X-ray and resistivity measurements. It was found that a multilayer microstructure forms below 600°C with an amorphous disilicide layer appearing between the Si substrate and a Ti_5Si_3 capping layer. At higher temperatures, the amorphous layer crystallizes into the C49 $TiSi_2$ phase, which transforms at another higher temperature to C54 $TiSi_2$. In some regions, the Ti_5Si_3 phase is found adjacent to the C54 $TiSi_2$ phase, suggesting that a template mechanism may be operating between the overlayer of Ti_5Si_3 and the underlayer of C49 $TiSi_2$, assisting its transformation to C54. Eventually, the Ti_5Si_3 layer is consumed by the formation of additional disilicide. A C40 disilicide phase was also observed at temperatures

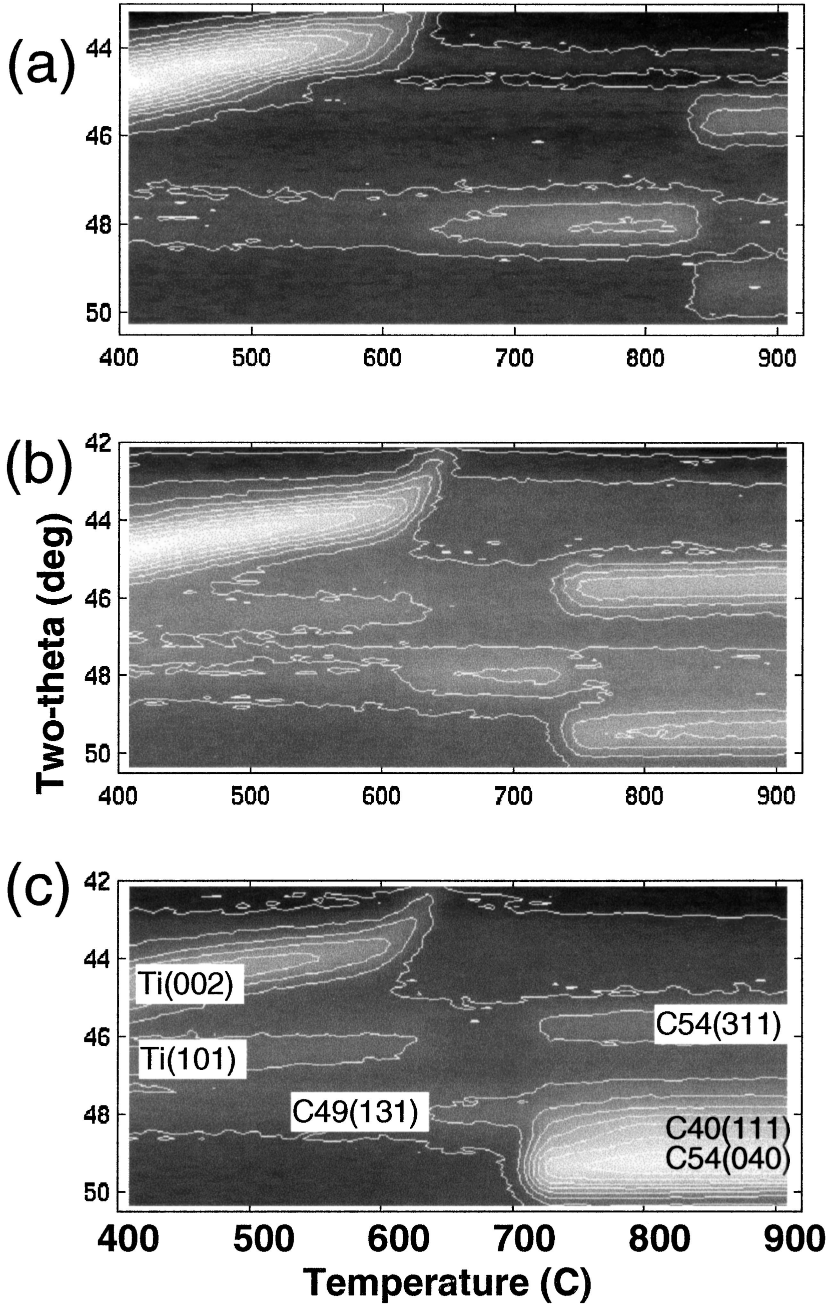

Figure 8 In situ X-ray diffraction patterns versus temperature for (*a*) Ti, (*b*) Ti(3.3 at% Ta), and (*c*) Ti(5.9 at% Ta) on poly-Si (19).

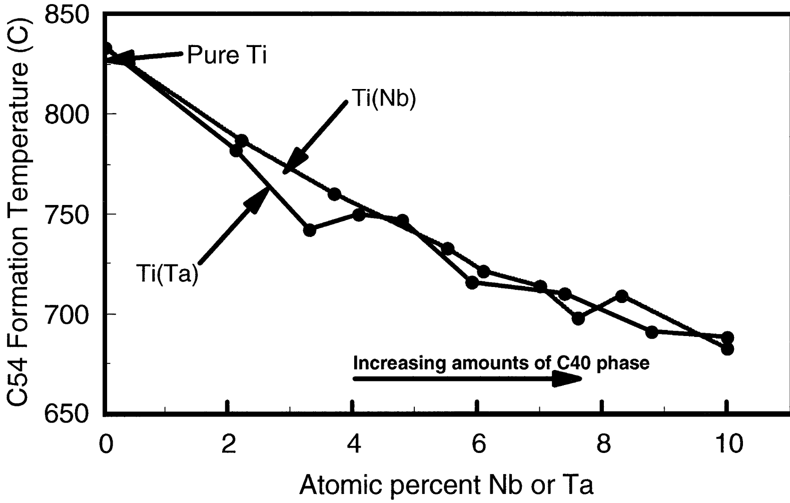

Figure 9 C49-to-C54 $TiSi_2$ transformation temperature versus at% Nb or Ta added to Ti (19).

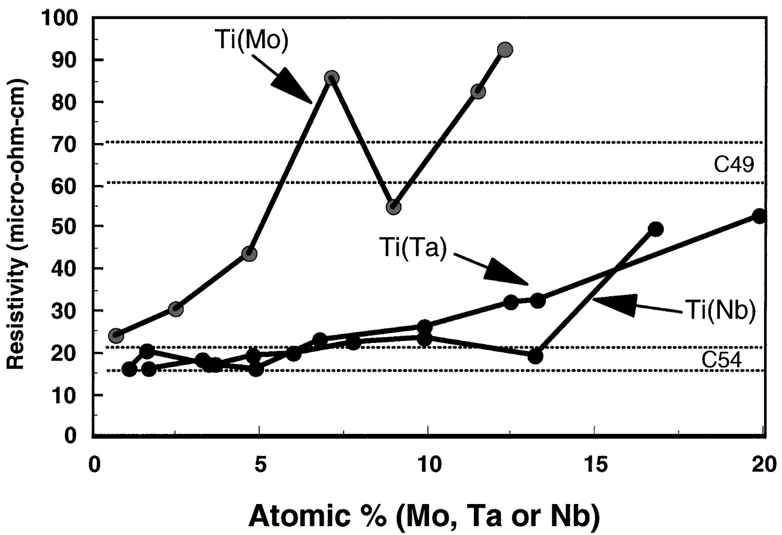

Figure 10 Resistivity versus at% Mo, Ta, or Nb in Ti reacted with Si. The resistivity ranges for C49 and C54 $TiSi_2$ are indicated (19).

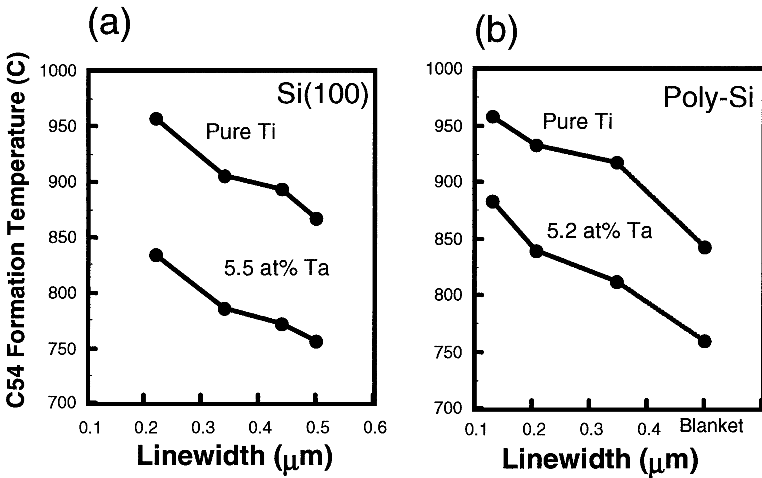

Figure 11 C54 $TiSi_2$ formation temperature versus line width for (*a*) Si(100) lines with Ti or Ti(5.5 at% Ta) and (*b*) poly-Si lines with Ti or Ti(5.2 at% Ta) (19).

above those required for C54 formation, presumably stabilized by the Ta content (31). However, in this case the C40 did not serve as a template for C54, because the C54 appears before the C40 phase.

DISCUSSION

When it was found that ion implantation of Mo into Si enhanced the formation of C54 $TiSi_2$, two mechanisms were immediately considered. The first mechanism is the reduction of grain size in the C49 phase, leading to a higher density of grain boundary triple points, which have been proposed as nucleation sites for the transformation to the C54 phase (32, 32a). Ma et al (32, 32a) had previously examined the grain structure of C49 $TiSi_2$ and estimated that 10–15% of the grain boundary triple points were providing nucleation sites for growth of the C54 phase. The precise structure of the nucleation sites has not been determined in this material, because the site density is very low and the nucleation regions are erased by the transformation to C54. However, each of the enhancement methods described in this review causes a pronounced reduction in grain size of the final C54 phase, by ~100-fold, providing evidence for this mechanism. Further studies of the microstructure associated with the C49-to-C54 transformation have shown that a nucleation site density of $\sim 0.1/\mu m^2$ is quite typical. Gignac et al (24) observed the grain sizes and nucleation site density by in situ TEM, whereas Privitera et al (33) obtained the nucleation site density from electrical measurements of various-size structures, and Quilici et al (34) determined the nucleation site density from

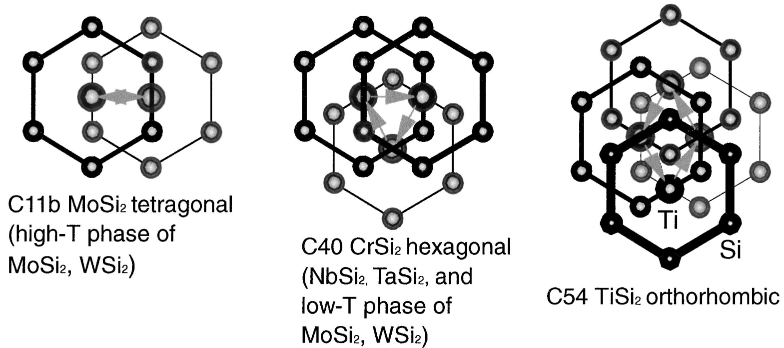

Figure 12 Lattice planes and stacking sequence of C11b, C40, and C54 disilicides.

Raman studies of the C54 phase. Taken together, these measurements show that the nucleation site density typically represents only a fraction of $\sim 10^{-4}$ of the grain boundary triple point density, not as high as the fraction of 10^{-1} previously reported (32). These low fractions suggest that nucleation sites must have very speci c microstructural features to initiate the growth of C54 grains.

The second mechanism immediately considered is the known similarity in crystal structures between the orthorhombic C54 $TiSi_2$ phase and both the tetragonal C11b and hexagonal C40 disilicide phases, depicted in Figure 12. Crystallites of C11b or C40 phases could provide template sites on which the barrier to nucleation of the C54 phase would be greatly reduced. Systematic measurements of silicide crystal structures have shown that many disilicide phases consist of a layered hexagonal (or almost hexagonal) structure (31, 35—37)The tetragonal C11b $MoSi_2$ structure is a two-layer (abab...) stacking of almost hexagonal metal disilicide planes and is the high temperature phase of $MoSi_2$ and WSi_2. The hexagonal C40 $CrSi_2$ structure is a three-layer (abcabc...) stacking of hexagonal metal disilicide planes and is found in $TaSi_2$, $NbSi_2$, and the low-temperature phase of $MoSi_2$ and WSi_2. The orthorhombic C54 $TiSi_2$ structure is a four-layer (abcdabcd...) stacking of almost hexagonal metal disilicide planes, and the similarity of this structure to C11b and C40 is much greater than to the orthorhombic C49 $ZrSi_2$ phase, which is a buckled structure. The phase diagrams of many metal alloy disilicides have been determined, and it is well established that C54 $TiSi_2$ that is alloyed with C40 metal disilicides such as WSi_2 has a wide range of single-phase C40 compositions and a small range of single-phase C54 compositions (31, 36). Two Ti(Mo)Si_2 compositions with the C40 structure are also documented (22). The atom spacings in the hexagonal layers of many metal alloy disilicide C40 phases are also close to those in the (040) plane of C54 $TiSi_2$, with a mismatch of only 0.3% for $TaSi_2$, for example (17). With this crystallographic information as background to these studies, a careful search for evidence of template phases has been made with both X-ray diffraction and TEM methods (16—1921, 24, 25, 25a, 28, 29, 38).

A significant challenge in identifying a template phase is that the template material may exist only briefly in the sequence of phase formation, being eventually consumed by the growth of the final phases. Clear identification therefore requires either quenching many samples from a narrow temperature range for detailed room temperature study or sensitive in situ phase identification methods that can provide structure information during heat treatment. In these silicide systems, both methods were needed, using temperature-ramped X-ray measurements to reveal the presence of phases and to narrow the range of compositions, heat treatments, and other parameters before undertaking extensive microstructure studies. Detailed TEM studies were essential in establishing direct evidence for template mechanisms, such as grain-to-grain relationships in the intermediate temperature regions of phase formation.

Based on X-ray diffraction measurements, the template role of C40 (Ti, Mo)Si_2 in Ti/Mo/Si interlayer samples was described by Mouroux et al (16), and the presence of the C40 phase was reported in Ti/Ta/Si interlayer samples (17) and in alloy samples of Ti(Mo), Ti(Ta), and Ti(Nb) (19). Kittl et al (25, 25a) reported TEM identification of $MoSi_2$ in Mo-implanted samples, along with Ti_5Si_4, Mo_5Si_3, and another phase related to Mo_5Si_3. Cheng et al (28) also reported the ternary C40 (Ti, Mo)Si_2 phase in Mo interlayer samples and used N_2 ion implantation to partially separate the effects of Mo-based templates and C49 grain size reduction. Their results indicate that the presence of Mo is more important than grain size reduction alone. Ohmi & Tung (29) also examined both Mo and amorphous $MoSi_x$ interlayers and favor grain size reduction as the main mechanism. Quintero et al (21) reported both C40 and Ti_5Si_3 phases in Ti(Ta) alloy samples. Although there have been suggestions that the C49 $TiSi_2$ phase is bypassed in some of these modified Ti/Si systems (25, 25a), in situ temperature-ramped studies have consistently shown evidence of C49 before C54 formation, although it may exist only in a narrow temperature range. One complicating factor is that the X-ray diffraction peaks for C49(131), C40(111), and Ti_5Si_3(211) lie very close to each other for these Ti alloys, and a clear separation of these phases needs additional diffraction peaks to be confirmed.

Microstructure measurements with TEM have provided significant details on the physical relationship of precursor phases and the C54 phase. In the study of Ti(Ta) alloy reactions with Si by Quintero et al described above (21), there is clear evidence for an amorphous disilicide layer adjacent to a layer of Ti_5Si_3, and then the C49, C54, and C40 disilicides appear in specific physical relationships to each other. This study strongly suggests a template relationship between the Ti_5Si_3 and C54 phases, which is supported by their small lattice mismatch and physical proximity (21). Also, the role of solid-state amorphization in the initial metal-Si mixing reaction needs further consideration (21, 39), because the subsequent evolution of crystalline phases can be complex, with multiple phases reported in close proximity in the Ti-Si system and other silicides (21, 39). Clearly, X-ray diffraction alone cannot confirm direct grain-to-grain orientation relationships and amorphous layer interactions, and more TEM examinations are needed to fully understand the template mechanisms in these closely related silicides.

Additional measurements that have provided insight into the mechanisms for C54 formation are the crystallographic texture distributions and in situ TEM observations of the moving C49-to-C54 transformation front. In the reaction of pure Ti with Si, a trend from (311) to increased (040) texture has been observed with decreasing film thickness and line width (40), presumably because of surface energy minimization as the surface-to-volume ratio is increased. Also, in-plane alignment of the C54 structure was found in very narrow patterned lines, with the C54(004) direction aligned with the patterned line direction, suggesting an anisotropic growth velocity of the phase boundary between growing C54 grains and the fine-grained C49 phase (41). In this latter experiment, the normal (040) texture also showed anisotropy relative to the line direction, indicating that the C54 grains had a greater angular range of tilt perpendicular to the line direction than along the line direction. These relationships are more consistent with an alignment mechanism based on growth rate anisotropy than with a mechanism based on sidewall nucleation. The in situ measurements (24) showed the transformation to be very sparsely nucleated, with a nucleation site density of $\sim 0.1/\mu m^2$, with the front moving at velocities of 0.5–1.0 μm/s at a temperature of 830°C in blanket and narrow-line samples. The motion appeared as a combination of rapid advances and pauses, as the front appeared temporarily pinned. Also, while some narrow lines underwent the transformation, neighboring lines were often observed to remain in the C49 phase. These observations support the earlier observations of sparse nucleation density (6) and small energy change (7) associated with the C49-to-C54 transformation. Although such detailed studies have not been reported in Ti/Si samples with implanted, interlayer, or alloy metal additives, such additional detail could help to distinguish between the mechanisms of reduced grain size and crystallograpic templates.

If reduced C49 grain size were the only mechanism enhancing C54 formation, then one would expect almost any additive metal or second-phase particle to have a similar effect. The published evidence shows, however, that the elements that most strongly enhance C54 $TiSi_2$ formation (Mo, W, Nb, and Ta) are grouped to the right of Ti in the periodic chart of the elements (Figure 13). Whereas many elements have been tested, only those with clear enhancement effects on C54 formation have been examined in detail, and a comprehensive evaluation of all possible additives has not been published.

Recent tight-binding calculations of the electron density of states in silicides by Bonoli et al (42) confirm the very small energy difference between C49 and C54 $TiSi_2$ (<50 meV/atom) and provide a clear understanding of the trend from C49 to C54 to C40 disilicides as the electron/atom ratio is increased. For example, increasing the number of electrons per formula unit from 12 to 13, equivalent to moving from $ZrSi_2$ to $NbSi_2$ (4 electrons per Si, 4 per Zr, and 5 per Nb), increases the total energy of C49 relative to C54 and lowers the total energy of C40 relative to C54. This trend originates in the rapidly increasing electron density of states at the Fermi level vs electron/atom ratio for the C49 structure and the more moderate increase for the C40 structure. This is exactly what is achieved by adding increasing concentrations of the elements highlighted in Figure 13 to Ti.

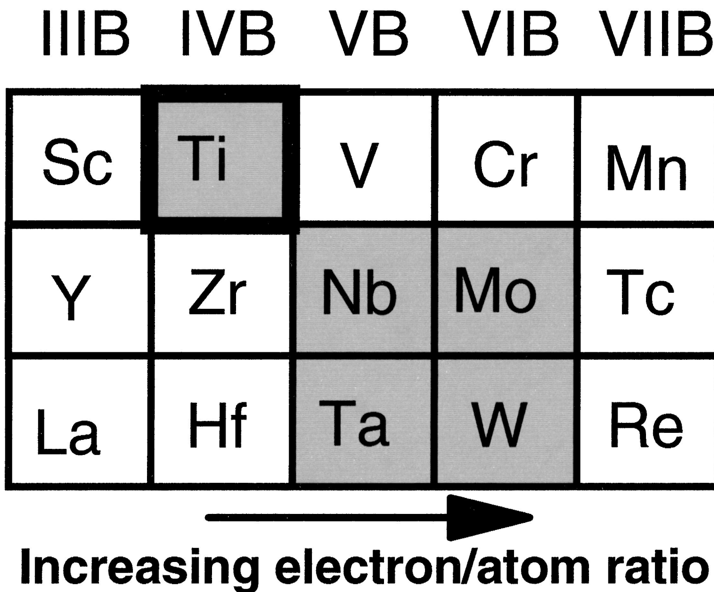

Figure 13 Elements near Ti in the periodic chart of the elements, showing the direction of increasing electron/atom ratio.

A supporting observation is that, by adding Al to the Ti/Si system (43), which decreases the electron/atom ratio, C49 is stabilized, and the C54 formation temperature is increased. Based on this trend, one expects that V and Cr should cause a similar enhancement to that observed for Mo, W, Nb, and Ta. This has not been confirmed, however, possibly because the smaller atomic size of V and Cr relative to Mo, W, Nb, and Ta should weaken the template effects of C40 VSi_2 and C40 $CrSi_2$.

The interplay of reactive-phase growth kinetics and thermodynamic-phase stability continues to challenge our ability to predict the behavior of metal silicide systems (44, 44a, 45), because we have the capability to calculate the relative energetics of crystalline phases (42), but not the full capability to predict the atomic motions that are required to obtain the necessary local concentrations. For example, the presence of additive metals retards the formation of the C49 phase in some of the systems discussed above, an effect that can be ascribed to the formation of a temporary diffusion barrier (18). The temperature for subsequent phase formation and interdiffusion is thereby increased, which changes the relative fluxes of metal and silicon atoms and also the relative stability of competing phases. Therefore, we can expect to continue to find subtle relationships between morphology and phase formation in multicomponent metal silicides, such as those observed by Quintero et al (21).

CONCLUSIONS

Three methods for introducing additive metals have been developed which enhance the formation of C54 $TiSi_2$ at lower temperatures and in narrower-line features than occur with the pure Ti/Si reaction. In each of these methods, there is evidence for decreased grain size of the precursor C49 $TiSi_2$ phase, and in some cases there is structural evidence for a crystallographic template mechanism. Both of these effects are expected to lower the barrier to nucleation of the C54 phase. The electronic origin of the stability trend from C49 to C54 to C40 structures with increasing electron/atom ratios supports the picture that the specific disilicides formed with Mo, W, Nb, and Ta are important in the enhancement mechanism. The large number of possible template phases includes disilicides of the C40 or C11b structure, alloy disilicides such as $(Ti,Mo)Si_2$ which may also have these structures, and the metal-rich phases including Ti_5Si_3, Ta_5Si_3, and their alloy counterparts. Because a template phase may have only a transitory existence, conclusive proof of the enhancement mechanisms has still not been obtained and probably involves aspects of both grain size reduction and template silicide phases. The relevance of this subject remains high as the semiconductor industry continues to shrink the size of silicon devices and their contacts, and a better understanding of compound phase formation in very small dimensions will be required for continued progress.

ACKNOWLEDGMENTS

The authors thank LA Clevenger, FM d'Heurte, L Gignac, J Jordan-Sweet, RA Roy, KL Saenger, GL Miles, RW Mann, J Nakos, SL Zhang, A Mourous, A Quintero, M Libera, V Svilan, and KF Ludwig, Jr., for fruitful collaborations and PD Agnello, KP Rodbell, R Viswanathan, and JB Lasky for insightful discussions. We thank the staffs of the IBM Advanced Lithography Facility, IBM Silicon Innovation Facility, IBM Burlington manufacturing line, and R. A. Carruthers for sample preparation. The National Synchrotron Light Source is supported by the U.S. Department of Energy, Division of Materials Science and Division of Chemical Sciences, under contract DOE #DE-AC02-76CH00016.

Visit the Annual Reviews home page at www.AnnualReviews.org

LITERATURE CITED

1. Mann RW, Clevenger LA, Agnello PD, White FR. 1995. *IBM J. Res. Dev.* 39:403
2. Semiconductor Industry Association. 1997. *National Technology Roadmap for Semiconductors*. San Jose, CA: Semiconductor Ind. Assoc
3. d'Heurle FM, Gas P, Engstrom I, Nygren S, Ostling M, Petersson CS, 1985. *IBM RC Report 11151*. Yorktown Heights, NY:IBM
4. Beyers R, Sinclair R.1985. *J. Appl. Phys.* 57:5240

5. Mann RW, Clevenger LA. 1994. *J. Electrochem. Soc.* 141:1347
6. Lasky J, Nakos J, Cain O, Geiss P. 1991. *IEEE Trans. Electron. Devices* 38:2629
7. Raaijmakers IJMM, Kim KB. 1990. *J. Appl. Phys.* 67:6255
8. Clevenger LA, Mann RW, Roy RA, Saenger KL, Cabral C Jr, Piccirillo J. 1994. *J. Appl. Phys.* 76:7874
9. Ohguro T, Nakamura S, Koike M, Morimoto T, Nishiyama A, et al. 1994. *IEEE Trans. Electron. Devices* 41:2305
9a. Clevenger LA, Harper JME, Cabral C Jr, Nobili C, Ottaviani G, Mann RW. 1992. *J. Appl. Phys.* 72:4978
10. Li XH, Carlsson RA, Gong SF, Hentzell HTG. *J. Appl. Phys.* 72:514
11. d'Heurle FM, Harper JME. 1990. *IBM Tech. Discl. Bull.* 33:7
12. Kuwano H, Phillips JR, Mayer JW. 1990. *Appl. Phys. Lett.* 56:440
13. Tung RT. 1996. *Mater. Res. Soc. Symp. Proc.* 402:101
14. Motakef S, Harper JME, d'Heurle FM, Gallo TA, Herbots N. 1991. *J. Appl. Phys.* 70:2660
15. Mann RW, Miles GL, Knotts TA, Rakowski DW, Clevenger LA, et al. 1995. *Appl. Phys. Lett.* 67:3729
15a. Clevenger LA, Mann RW, Miles GL, Harper JME, d'Heurle FM, et al. 1995. *Proc. VLSI Multilevel Interconnection Conf., Santa Clara, CA,* p. 626. Pittsburgh: Mater. Res. Soc.
16. Mouroux A, Zhang SL, Kaplan W, Nygren S, Ostling M, Petersson CS. 1996. *Appl. Phys. Lett.* 69:975
17. Mouroux A, Zhang SL, Petersson CS. 1997. *Phys. Rev. B* 56:10614
18. Cabral C Jr, Clevenger LA, Harper JME, d'Heurle FM, Roy RA, et al. 1997. *J. Mater. Res.* 12:304
19. Cabral C Jr, Clevenger LA, Harper JME, d'Heurle FM, Roy RA, et al.1997. *Appl. Phys. Lett.* 71:3531
20. Cabral C Jr, Clevenger LA, Stephenson GB, Brauer S, Morales G, Ludwig KF Jr. 1995. *Mater. Res. Soc. Symp. Proc.* 375:253
21. Quintero A, Libera M, Cabral C Jr, Lavoie C, Harper JME. 1999. *J. Mater. Res.* 14:4690
22. JCPDS-International Center for Diffraction Data, PDF-2 Database. 1990. Newton Square, PA: JCPDS
23. Centre Interdepartmental de Microscopie Electronique.1998. *EMS Online*. http://cimewww.epfl.ch
24. Gignac LM, Svilan V, Clevenger LA, Cabral C Jr, Lavoie C. 1997. *Proc. Mater. Res. Soc.* 441:255
25. Kittl JA, Hong QZ, Rodder M, Prinslow DA, Misium G. 1996. *VLSI Tech. Dig.* 14:1
25a. Kittl JA, Hong QZ, Yang H, Yu N, Samavedam SB, Gribelyuk MA. 1998. *Thin Solid Films* 332:404
25b. Gribelyuk MA, Kittl JA, Samavedam AB. 1999. *J. Appl. Phys.* 86:2571
26. Maex K. 1993. *Mater. Sci. Eng.* R11:50
26a. Hewett CA, Lau SS, Suni I, Poker DB. 1985. *Nucl. Instrum. Methods B* 7/8:597
27. Saenger KL, Cabral C Jr, Clevenger LA, Roy RA. 1997. *Proc. Mater. Res. Soc. Adv. Metall. ULSI Appl., 1996. ULSI XII, San Francisco*, p. 203. Pittsburgh: Mater. Res. Soc.
28. Cheng SL, Jou JJ, Chen LJ, Tsui BY. 1999. *J. Mater. Res.* 14:2061
29. Ohmi SI, Tung RT. 1999. *Proc. Mater. Res. Soc. Fall 1998.* In press
30. Quintero A, Libera M, Cabral C Jr, Lavoie C, Harper JME. 1998. *Microsc. Microanal.* 4(Suppl. 2):666
31. Goldschmidt HJ. 1967. *Interstitial Alloys*, p. 322. New York: Plenum
32. Ma Z, Xu Y, Allen LH, Lee S. 1993. *J. Appl. Phys.* 74:2954
32a. Ma Z, Allen LH, Allman DDJ. 1995. *J. Appl. Phys.* 77:4384
33. Privitera S, La Via F, Grimaldi MG, Rimini E. 1998. *Appl. Phys. Lett.* 73:3863
34. Quilici S, Meinardi F, Sabbadini A. 1999. *Solid State Commun.* 109:141

35. d'Heurle FM. 1982. In *VLSI Science and Technology*, ed. C Dell'Oca, WM Bullis, p. 194. Pennington, NJ: Electrochem. Soc.
36. Gas P, Tardy FJ, d'Heurle FM. 1986. *J. Appl. Phys.* 60:193
37. Maex K, Van Rossum M, eds. 1995. *Properties of Metal Silicides*. London: INSPEC
38. Zhang SL, Lavoie C, Cabral C Jr, Harper JME, d'Heurle FM, Jordan-Sweet JL. 1999. *J. Appl. Phys.* 85:2617
39. Chen LJ, Hsieh WY, Lin JH, Lee TL, Chen JF, et al. 1994. *Proc. Mater. Res. Soc.* 320:343
40. Roy RA, Clevenger LA, Cabral C Jr, Saenger KL, Brauer S, et al. 1995. *Appl. Phys. Lett.* 66:1732
41. Svilan V, Rodbell KP, Clevenger LA, Cabral C Jr, Roy RA, et al. 1997. *J. Electron. Mater.* 26:1090
42. Bonoli F, Iannuzzi M, Miglio L, Meregalli V. 1998. *Appl. Phys. Lett.* 73:1964
43. Zhang SL, d'Heurle FM, Lavoie C, Cabral C Jr, Harper JME. 1998. *Appl. Phys. Lett.* 73:312
44. d'Heurle FM, Gas P. 1986. *J. Mater. Res.* 1:1
44a. d'Heurle FM. 1988. *J. Mater. Res.* 3:167
45. Ottaviani G. 1986. *Thin Solid Films* 140:3